

GW quasiparticle band gap of the hybrid organic-inorganic perovskite $\text{CH}_3\text{NH}_3\text{PbI}_3$: Effect of spin-orbit interaction, semicore electrons, and self-consistency

Marina R. Filip and Feliciano Giustino

Department of Materials, University of Oxford, Parks Road, Oxford OX1 3PH, United Kingdom

We study the quasiparticle band gap of the hybrid organic-inorganic lead halide perovskite $\text{CH}_3\text{NH}_3\text{PbI}_3$, using many-body perturbation theory based on the *GW* approximation. We perform a systematic analysis of the band gap sensitivity to relativistic spin-orbit effects, to the description of semicore Pb-5*d* and I-4*d* electrons, and to the starting Kohn-Sham eigenvalues. We find that the inclusion of semicore states increases the calculated band gap by 0.2 eV, and self-consistency on the quasiparticle eigenvalues using a scissor correction increases the band gap by 0.4 eV with respect to the G_0W_0 result. These findings allow us to resolve an inconsistency between previously reported *GW* calculations for $\text{CH}_3\text{NH}_3\text{PbI}_3$. Our most accurate band gap is 1.65 eV, and is in good agreement with the measured optical gap after considering a small excitonic shift as determined in experiments.

PACS numbers: 71.15.Mb, 71.20.Nr, 71.70.Ej, 71.15.Qe

I. INTRODUCTION

The development of solar cells based on metal-halide perovskites has shown unprecedented progress since perovskite absorbers were first reported in 2009.¹ In less than five years the power conversion efficiency of perovskite cells has increased from 3.8%¹ to the current record of 19.3%.² Photovoltaic devices based on methylammonium (CH_3NH_3^+ , MA) lead halide, MAPbI_3 and MAPbBr_3 , were originally fabricated using a dye-sensitized solar cell architecture.³ In this device setup the electrons generated upon absorption of light in the perovskite are collected in a TiO_2 electron acceptor, while the hole is regenerated by a redox couple in an electrolytic solution.¹ After replacing the liquid electrolyte by the solid-state hole-transporter spiro-MeOTAD, the efficiency of these solar cells increased above 10%.^{4,5} This breakthrough generated a surge of interest in perovskites within the solar cell community.^{6,7} Further increase in the efficiency was achieved by improving fabrication techniques,^{2,8,9} and by exploring mixed metal-halide perovskites.¹⁰

In view of large-scale industrial manufacturing of perovskite-based solar cells, several avenues of development are actively being explored. Ambipolar charge transport in the perovskite layer was demonstrated by the successful development of simple planar heterojunction solar cells.^{11–19} Control of the color of the devices^{10,20,21} as well as partial transparency^{20,22} were also achieved. Flexible thin film perovskite solar cells have been fabricated via low-temperature processing.^{12,14,23–25} Toxicity concerns have also been addressed by studying alternatives to Pb such as Sn-based mixed-halide perovskite solar cells.^{26,27}

In parallel with these rapid technological advances, significant efforts are currently being devoted to understanding the microscopic mechanisms which are responsible for the exceptional performance of these hybrid perovskites. MAPbI_3 belongs to the family of ABX_3 perovskites. The Pb and I atoms form a three-dimensional

network of corner-sharing octahedra, with the Pb atoms occupying the center of each octahedron and the I atoms located at its corners. In this configuration the Pb-I network encloses a cuboctahedral cavity, with the MA cation located at its center (Fig. 1). The crystal structure of metal-halide perovskites is strongly dependent on temperature^{28–30} and undergoes two phase transitions. At low temperature, the crystal structure of MAPbI_3 is orthorhombic and the MA cations have a well-defined orientation within the cuboctahedral cavity.^{28–30} Above 162 K the Pb-I network undergoes a phase transition to a tetragonal structure²⁹, and above 327 K the system stabilizes in its most symmetric cubic perovskite structure.²⁹ As the temperature increases the MA cation

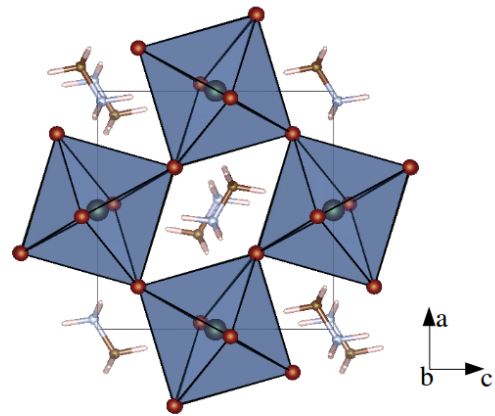


FIG. 1: Polyhedral representation of the crystal structure of MAPbI_3 . The Pb atoms are represented by the large blue spheres at the center of each octahedron. The small red spheres located at the shared corners of the octahedra are the I atoms. The MA cations are shown using ball-and-stick models at the center of the cuboctahedral cavities (C is light blue, N is brown, H is pink). The structure is viewed along the *b* lattice vector.

becomes orientationally disordered. The structure of the Pb-I network in MAPbI₃ has been studied in detail for each phase using temperature dependent X-ray diffraction (XRD).^{29,30} These studies also noted structural anomalies relating to the position of the apical I atoms, as well as possible intermediate phases.^{29,30}

Given the uncertainties in the structure of the room-temperature tetragonal phase, in this work we focus on the low-temperature orthorhombic structure of MAPbI₃. The space group of this system is *Pnma* and the orientation of the MA cations is well understood.^{28–30} Accurate experimental measurements of the optical band gap of the low-temperature phase of MAPbI₃ have been reported for temperatures down to 4 K.³¹

The optical band gap of metal-halide perovskites can be broadly tuned by manipulating their chemical composition and crystal structure.^{21,29,30,32–37} The gap can be tuned from 1.17 eV to 1.55 eV by controlling the mixing fraction of Pb and Sn in MAPb_xSn_{1-x}I₃.^{30,38} Perovskites based on alternative cations such as Cs and formamidinium, HC(NH₂)₂⁺, or on mixes of different cations showed a tunable optical onset, spanning a range of 0.25 eV.^{33,35,36} Recently our computational study of the steric effect of the cation highlighted that the band gap could be finely tuned over a wide range by considering new cations not studied hitherto.³⁷ The band gap can also be tuned by exchanging the halide for Cl or Br.^{10,20,21} This possibility has led to band gap tunability in the range 1.5 eV to 2.3 eV.

MAPbI₃ is a semiconducting material, with an optical band gap of ~1.6 eV at room temperature.²⁹ Optical absorption spectra measured as a function of temperature identified a weakly bound exciton, with a binding energy estimated in the range 55 ± 20 meV.³¹ By applying the law of mass action for Wannier excitons the authors of Ref. 31 concluded that at room temperature free carriers dominate over excitons in MAPbI₃. In addition it is now understood that both electrons and holes have very long diffusion lengths, reaching up to 1 μm.^{39–43} Therefore it appears that MAPbI₃ perovskite share important similarities with standard tetrahedral semiconductors such as GaAs, and this may partly account for their extraordinary performance.^{31,44–46}

Computational studies of metal-halide perovskites within density functional theory (DFT)⁴⁷ have explored a variety of electronic and structural properties. In particular, perovskites with mixed I and Cl halides have been investigated, highlighting the role of Cl incorporation in the structural and electronic properties of bulk MAPbI_{3-x}Cl_x,⁴⁸ and the interface between TiO₂ and MAPbI_{3-x}Cl_x or MAPbI₃.^{49–51} The role of the cation as a spacer in the Pb-I network was established in computational studies of metal-halide perovskites.^{34,37} In particular, the size of the cation is understood to determine the volume and the structure of the cuboctahedral cavity.^{34,37,52,53} The effect of the orientation of MA has been studied in relation to UV/Vis absorption and Raman spectra,^{54,55} and a link with the hysteresis effect ob-

served in the electrical measurements of perovskite-based solar cells has been suggested.⁵⁶

DFT calculations of the band structure of MAPbI₃ revealed that the fundamental band gap is direct and located at the zone center. The valence band top and the conduction band bottom are predominantly of I-5*p* and Pb-6*p* character, respectively.^{29,37,46,49,57} The electronic states associated with the MA cation are located more than 5 eV away from the band edges, therefore they are not directly involved in the optical absorption onset.^{37,49} The band gap calculated using scalar relativistic DFT is surprisingly close to the measured optical gap.^{53,57–60} However, after incorporating spin-orbit interactions using fully relativistic DFT calculations, the gap becomes about 1 eV smaller than in experiments.^{59,60}

The significant discrepancy between fully-relativistic DFT band gaps and experimental optical gaps provided motivation for carrying out more sophisticated *GW* quasiparticle calculations.⁶¹ So far two studies addressed the quasiparticle band gap of MAPbI₃ within the *GW* approximation, using different approaches.^{58,62} Ref. 58 reported a quasiparticle band gap of 1.67 eV obtained within the G_0W_0 approximation. In this work the authors used a scalar relativistic approximation for the screened Coulomb interaction W_0 , and spin-orbit effects were included only in the Green's function G_0 as a correction term. Ref. 62 reported a G_0W_0 quasiparticle gap of 1.27 eV when spin-orbit coupling was fully included in the calculation of both G_0 and W_0 . Ref. 62 also calculated the quasiparticle band gap using the 'quasiparticle self-consistent *GW*' (QS*GW*) approach.⁶³ Surprisingly they report a QS*GW* band gap of 1.67 eV which matches the G_0W_0 results obtained in Ref. 58.

The present work was motivated by the difficulty in reconciling the findings of Refs. 58 and 62. Our aim was to understand the discrepancy between the G_0W_0 band gaps calculated in Refs. 58,62, and also to perform a sensitivity analysis of the band gap on the various approximations involved in *GW* calculations. In particular we investigated the effect of spin-orbit coupling both in the DFT and in the *GW* band gaps, by comparing scalar relativistic and fully relativistic calculations. We studied the effect of the semicore *d* electrons of Pb and I on the calculated *GW* band gaps. And we checked the numerical convergence of the band gap with respect to the cutoff on the number of empty states used in the Green's function and in the polarizability, with respect to the planewaves cutoff of the polarizability, and the Brillouin zone sampling.

Importantly we found that our best-converged, fully-relativistic G_0W_0 calculations yield a band gap which is about 0.4 eV smaller than the measured optical gap. In order to improve the agreement with experiment, we tested whether a simple self-consistent scissor-correction approach would increase the band gap, in the same spirit as *GW*+U calculations.^{64,65} Using this procedure we obtained a band gap of 1.65 eV, in very good agreement with experiment and with the calculations of Refs. 58,62.

We rationalize this result by arguing that, in the case of MAPbI₃, the self-consistent scissor correction is effectively equivalent to performing quasi-particle self-consistent *GW* as in Refs. 62, or to using the scalar relativistic *W* as in Refs. 58.

The manuscript is organized as follows. In Sec. II we briefly summarize the *GW* formalism, and indicate how we perform self-consistent scissor calculations. In Sec. III we describe our computational setup and analyze the numerical convergence of the band gap with empty states, planewaves cutoff, and Brillouin zone sampling. Our main findings are presented in Sec. IV. In Sec. V we discuss our results in relation to experiments and to the previous *GW* calculations of Refs. 58 and 62. In Sec. VI we offer our conclusions and identify important avenues for future research.

II. METHODOLOGY

A. Standard G_0W_0 method

Within *GW* many-body perturbation theory the quasi-particle energies are written as:^{61,66,67}

$$E_{n\mathbf{k}} = \varepsilon_{n\mathbf{k}} + Z(\varepsilon_{n\mathbf{k}}) \langle n\mathbf{k} | \hat{\Sigma}(\varepsilon_{n\mathbf{k}}) - V_{xc} | n\mathbf{k} \rangle, \quad (1)$$

where $|n\mathbf{k}\rangle$ denotes a Kohn-Sham state with band index n and crystal momentum \mathbf{k} , and $\varepsilon_{n\mathbf{k}}$ its corresponding eigenvalue. In Eq. (1) $\hat{\Sigma}(\omega)$ is the self-energy at the energy ω , $Z(\omega) = (1 - \partial \text{Re} \Sigma / \partial \omega)^{-1}$ is the quasiparticle renormalization, and V_{xc} is the DFT exchange and correlation potential. The self-energy is calculated in the G_0W_0 approximation as $\hat{\Sigma} = iG_0W_0$.^{66,67} Here G_0 is the non-interacting single particle Green's function, as obtained from the Kohn-Sham eigenstates. The screened Coulomb interaction is given by $W_0 = \epsilon^{-1}v$, with v the bare Coulomb interaction and ϵ^{-1} the inverse dielectric matrix. The dielectric matrix is calculated in reciprocal space as:

$$\epsilon_{\mathbf{G}\mathbf{G}'}(\mathbf{q}, \omega) = \delta_{\mathbf{G}\mathbf{G}'} - v(\mathbf{q} + \mathbf{G})P_{\mathbf{G}\mathbf{G}'}(\mathbf{q}, \omega), \quad (2)$$

where \mathbf{G} and \mathbf{G}' are reciprocal lattice vectors, \mathbf{q} is a wave vector in the first Brillouine zone, and $P_{\mathbf{G}\mathbf{G}'}(\mathbf{q}, \omega)$ is the polarizability in the random phase approximation (RPA).^{66,68,69} In order to describe the frequency-dependence of the dielectric matrix we use the Godby-Needs plasmon pole model.^{67,70,71} In this approximation the dielectric matrix is written as:

$$\epsilon_{\mathbf{G}\mathbf{G}'}(\mathbf{q}, \omega) = \delta_{\mathbf{G}\mathbf{G}'} + \frac{\Omega_{\mathbf{G}\mathbf{G}'}^2(\mathbf{q})}{\omega^2 - [\omega_{\mathbf{G}\mathbf{G}'}(\mathbf{q}) - i\eta]^2}, \quad (3)$$

where η is a small constant. The plasmon-pole parameters $\Omega_{\mathbf{G}\mathbf{G}'}^2$ and $\omega_{\mathbf{G}\mathbf{G}'}$ are obtained by evaluating the RPA dielectric matrix at $\omega = 0$ and at $\omega = i\omega_p$, ω_p being the plasma frequency.^{66,67,70,72} When performing convergence tests it is useful to partition the self-energy

into an energy-independent term, the exchange self-energy $\hat{\Sigma}_x$, and an energy-dependent term, the correlation self energy $\hat{\Sigma}_c$.

B. Self-consistent scissor correction

The G_0W_0 quasiparticle energies can be sensitive to the Kohn-Sham eigenvalues and eigenstates used as the starting point to calculate the perturbative corrections via Eq. (1).^{63–65,73–76} It is now well established that this sensitivity can be mitigated by employing a self-consistent approach in the many body perturbation theory problem, either by iteratively improving G and/or W , or by modifying the DFT starting point. Several approaches with varying levels of sophistication have been proposed to this effect.^{63–65,75,76}

In this study we test the use of a simple scissor correction approach in order to study the impact of self-consistency on the quasiparticle band gap of MAPbI₃. The scissor correction is particularly appropriate for MAPbI₃ since the optical absorption onset results from transitions between two parabolic bands which are well separated from other bands, therefore the effects of band mixing via off-diagonal matrix elements of the self-energy are expected to be very small.

In this approach we first determine the G_0W_0 band gap correction Δ using Eq. (1). Subsequently we repeat the *GW* calculation, after having applied a scissor correction of magnitude Δ to the conduction bands. This procedure is repeated until the correction $\Delta^{(i)}$ and $\Delta^{(i+1)}$ at two subsequent iterations i and $i+1$ are the same within a set tolerance. The scissor correction modifies both the Green's function G_0 and the screened Coulomb interaction W_0 via the RPA polarizability. For definiteness in the following we will refer to this approach as ‘SS-*GW*’ (self-consistent scissor *GW*).

The effect of the scissor correction can be seen as if obtained by adding a non-local exchange and correlation potential to the original Kohn-Sham Hamiltonian, $\hat{V}_{nl} = \Delta \hat{P}_c$, with \hat{P}_c being the projector on the manifold of unoccupied states. In order to avoid double-counting this extra potential must be removed from Eq. (1); we obtain:

$$E_{n\mathbf{k}} = \varepsilon_{n\mathbf{k}} + Z(\varepsilon_{n\mathbf{k}}) \langle n\mathbf{k} | \hat{\Sigma}(\varepsilon_{n\mathbf{k}}) - (V_{xc} + \hat{V}_{nl}) | n\mathbf{k} \rangle. \quad (4)$$

In this form the analogy with other techniques, such as $GW+U$ ^{64,65} or quasi-particle self-consistent *GW*⁶³ becomes evident. The main difference with more sophisticated approaches is that Eq. (4) is extremely easy to implement as a post-processing operation, and its effect on the quasiparticle corrections is transparent.

We note in passing that the scissor-corrected *GW* self-energy has a well-defined upper bound. In fact, if we consider the limit of large Δ we find that the RPA dielectric matrix becomes the identity, therefore the self-energy reduces to G_0v . After separating the Green's function

into its analytic and non-analytic components and noting that the frequency convolution of the analytic part vanishes,⁷⁷ we obtain that for $\Delta \rightarrow \infty$ the self-energy and the renormalization factor tend to $\hat{\Sigma} = \hat{\Sigma}_x$ and $Z = 1$, respectively.

This indicates that the scissor correction only affects the correlation self-energy Σ_c , and acts to improve the description of the screening via a modulation of the band gap.

It goes without saying that one could replace \hat{V}_{nl} by more advanced options, such as for instance hybrid functional with varying fractions of exchange.^{78,79} However here for the sake of simplicity we do not explore these alternatives.

III. COMPUTATIONAL SETUP

A. DFT calculations

All DFT calculations are performed using the **Quantum ESPRESSO** software package⁸⁰ within the local density approximation (LDA).^{81,82} For C, N and H we use non-relativistic, norm-conserving von Barth-Car⁸³ pseudopotentials from the **Quantum ESPRESSO** pseudopotential library. For Pb and I we generate two sets of Troullier-Martins⁸⁴ norm conserving, fully relativistic pseudopotentials using the `ld1.x` pseudopotential generation tool of the **Quantum ESPRESSO** suite. We consider the following valence atomic configurations: Pb without ($6s^26p^2$) or with semicore states ($5d^{10}6s^26p^2$), I without ($5s^25p^3$) or with semicore states ($4d^{10}5s^25p^3$). The total energy is converged within 6 meV/atom using a planewaves kinetic energy cutoff of 100 Ry for the calculations without I-4d semicore electrons. In order to achieve the same level of convergence in the presence of I-4d states we employ a cutoff of 150 Ry. Self-consistent calculations are performed using a $6 \times 6 \times 6$ Γ -centered Brillouine zone grid, comprising of 112 irreducible points.

In order to describe the low-temperature phase of MAPbI₃ we consider an orthorhombic unit cell including 4 formula units (48 atoms). In all our calculations we use the atomic positions and lattice parameters obtained in our previous work³⁷ by performing a complete structural optimization starting from the XRD data of Ref. 29.

B. G_0W_0 calculations

All the GW calculations are performed using version 3.4.1 of the **Yambo** software package⁸⁵, which includes relativistic spin-orbit coupling within the GW implementation.^{86–88}

Plasmon pole approximation – In order to check whether the plasmon-pole approximation in Eq. (3) is adequate for MAPbI₃ we check the sensitivity of the calculated band gap to the plasmon pole parameter ω_p . To this

aim we perform G_0W_0 calculations using $\omega_p = 7, 14, 20, 27,$ and 34 eV. The corresponding variation of the gap is found to be at most 10 meV, suggesting that the dynamical screening is correctly described. These tests correspond to scalar-relativistic calculations in the absence of semicore electrons, using 240 unoccupied states, kinetic energy cutoffs of 136 eV and 54 eV for the exchange and correlation parts of the self-energy, respectively, and an unshifted $2 \times 2 \times 2$ Brillouin zone grid.

Brillouin zone sampling – We test the convergence of the quasiparticle band gap with respect to the sampling of the Brillouin zone used in the convolution of G and W by comparing the band gaps obtained using unshifted $2 \times 2 \times 2, 3 \times 3 \times 3$ and $4 \times 4 \times 4$ meshes (with 8, 14, and 36 irreducible \mathbf{k} -points, respectively). The band gap is found to change by less than 10 meV throughout. These tests were carried out using the same parameters reported in the previous paragraph.

Unoccupied states – Since the planewaves kinetic energy cutoff for the polarizability and the number of unoccupied states depend on whether we include semicore d states in our calculations, we study the convergence for all four combinations of pseudopotentials for Pb and I, as described in Sec. III A. For completeness we carry out these tests both for scalar-relativistic (SR) and for fully relativistic (FR) calculations. In total we consider 8 scenarios, as shown in Fig. 2.

In order to determine optimal cutoff parameters we perform convergence tests for Σ_x and Σ_c separately. We found that a cutoff of 136 eV is sufficient to achieve convergence for Σ_x in all cases.

In the case of Σ_c we test the convergence of the band gap with the number of empty states, for polarizability cutoffs ranging from 14 to 82 eV for all cases. We define an energy cutoff for the unoccupied states using the energy of the highest state at Γ , relative to the valence band top. As a reference, the rightmost datapoints in Fig. 2(a) and (c) correspond to 1000 bands in total.

In the case of SR calculations the quasiparticle band gaps are converged with respect to the number of unoccupied states using a cutoff of 50 eV, corresponding to 1000 bands.

In the case of FR calculations the number of unoccupied states that need to be evaluated doubles with respect to SR calculations. This can be seen in Fig. 2(a) and (c), where 1000 states correspond to a cutoff of 30 eV and 55 eV in the FR and SR cases, respectively. This poses in principle a limit on how far we can push the convergence of FR band gaps. However from Fig. 2 we can see that the SR and FR curves follow very similar trends. This is expected given that the same pseudopotentials are used for both sets of calculations. By comparing the convergence trends in the SR and FR cases we estimate that the fully-relativistic gaps calculated for the rightmost points in Fig. 2(c) are converged within less than 0.1 eV in all cases.

Polarizability cutoff – The convergence of the band gap with respect to the polarizability cutoff is shown in

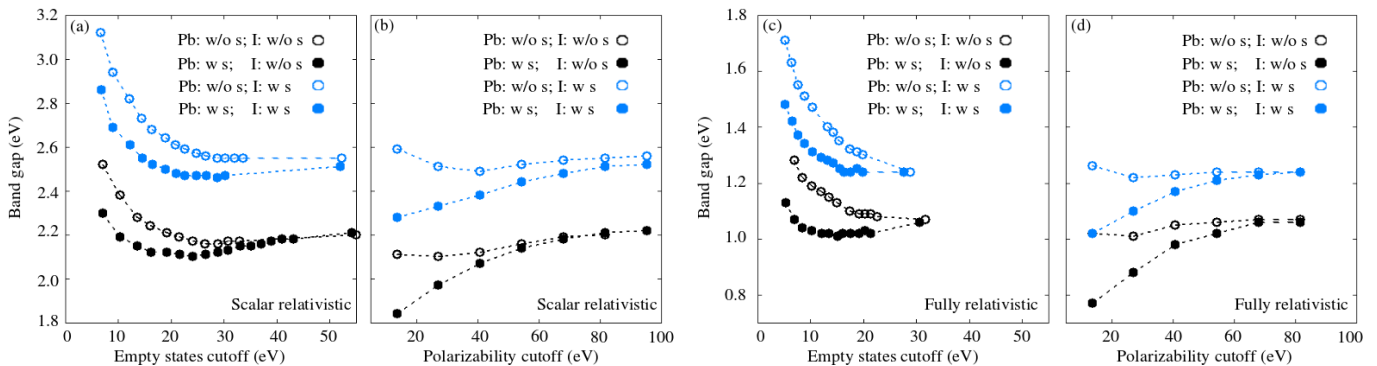


FIG. 2: Convergence of the quasiparticle band gap of MAPbI₃ with respect to the energy cutoff for unoccupied states [(a) and (c)], and with respect to the plane waves kinetic energy cutoff for the polarizability [(b) and (d)]. Panels (a) and (b) refer to SR calculations, while (c) and (d) are for FR band gaps. In each panel we show results for all four combinations of pseudopotentials considered here: Pb and I without semicore states (‘w/o s’, black empty circles), Pb with semicore (‘w s’) and I without semicore states (black filled circles), Pb without semicore and I with semicore states (blue empty circles), Pb and I with semicore states (blue filled circles). These data correspond to a $2 \times 2 \times 2$ Γ -centered Brillouin zone mesh, and a 136 eV plane waves cutoff for the exchange self-energy. The plane waves cutoff for the polarizability in panels (a) and (c) is set to 82 eV, and the number of total bands in (b) and (d) is set to 1000.

Fig. 2(b) and (d). The calculations are performed using 1000 bands in all cases. In order to contain the computational effort we tested cutoffs up to 95 eV in the SR case and 82 eV in the FR case. In all cases considered the quasiparticle band gaps appear converged when using a polarizability cutoff of 82 eV.

Having performed a detailed analysis of each convergence parameter, for the sake of clarity and reproducibility in the remainder of the manuscript we report quasiparticle band gaps calculated using the following setup: plane waves kinetic energy cutoff for the exchange and the correlation self-energies: 136 eV and 82 eV, respectively; total number of bands: 1000; plasmon pole parameter: $\omega_p = 27$ eV; Brillouin zone sampling: $2 \times 2 \times 2$ unshifted mesh.

IV. RESULTS

A. Effect of spin-orbit coupling

Table I shows a comparison between DFT/LDA and G_0W_0 calculations of the band gap of MAPbI₃ within both the scalar-relativistic and fully relativistic frameworks. The spin-orbit coupling is seen to induce a 0.9 eV red-shift of the DFT band gap, in agreement with previous reports.^{59,60}

Moving on to the GW quasiparticle corrections, we note that the red-shift induced by the spin-orbit coupling increases slightly and ranges between 1.1 and 1.3 eV. Our results are in line with the G_0W_0 calculations of Ref. 62, where a quasiparticle spin-orbit coupling correction of 1.5 eV was reported.

Table I also shows that our calculated quasi-particle band gap including spin-orbit corrections and semicore electrons is 1.24 eV. This value underestimates the measured

optical gap by approximately 0.4 eV,²⁹ suggesting that a perturbative treatment of the quasiparticle corrections is insufficient in the study of MAPbI₃. We will come back to this aspect in Sec. IV C.

Interestingly G_0W_0 calculations starting from the DFT/LDA states without including spin-orbit effects yield a very large gap of 2.51 eV, therefore they overestimate the measured optical gap by as much as 0.9 eV (Table I). This observation reinforces the point on the importance of relativistic spin-orbit corrections in this system.⁵⁹

B. Effect of semicore electrons

Table I shows that the DFT/LDA band gap for MAPbI₃ changes by less than 0.04 eV upon the inclusion of the Pb-5*d* and I-4*d* semicore electrons in the valence. By contrast, the quasiparticle band gap appears sensitive to the Pb-5*d* and I-4*d* states: upon inclusion of these states the band gap increases by up to 0.17 eV in the case of fully relativistic calculations. This trend can also be seen in the convergence study shown in Fig. 2. A significant fraction of this shift arises from the inclusion of I-4*d* states, as can be seen in the fifth line of Table I. The effect appears to be mostly associated with a blue-shift of the conduction band bottom upon inclusion of the I semicore electrons, as it is clearly seen in Fig. 3(a).

The effect of semicore electrons on the calculation of quasiparticle energies is well documented in literature.^{89–91} Usually this effect results from an additional exchange contribution to the self-energy, which results from the spatial overlap of diffuse semicore states with the valence states at the band edges. At variance with the exchange self-energy, the correlation part is less affected since the contribution of the semicore states is

		DFT/LDA				G_0W_0			
		Pb: w/o s	Pb: w s	Pb: w/o s	Pb: w s	Pb: w/o s	Pb: w s	Pb: w/o s	Pb: w s
		I: w/o s	I: w/o s	I: w s	I: w s	I: w/o s	I: w/o s	I: w s	I: w s
Γ_v	SR	0.00	0.00	0.00	0.00	-0.30	-0.31	-0.45	-0.53
	FR	0.00	0.00	0.00	0.00	0.06	0.09	0.12	0.14
Γ_c	SR	1.43	1.42	1.51	1.50	1.90	1.90	2.10	1.98
	FR	0.54	0.52	0.60	0.58	1.13	1.15	1.36	1.38
Gap	SR	1.43	1.42	1.51	1.50	2.20	2.21	2.55	2.51
	FR	0.54	0.52	0.60	0.58	1.07	1.06	1.24	1.24
	Difference	0.89	0.90	0.91	0.92	1.13	1.15	1.31	1.27

TABLE I: DFT/LDA Kohn-Sham energies and G_0W_0 quasiparticle energies of the valence band top (Γ_v), conduction band bottom (Γ_c), and band gap of MAPbI₃. We report the results of scalar relativistic calculations (SR) and fully relativistic calculations (FR) for all combinations of Pb and I pseudopotentials considered in this work ('w s'/'w/o s' indicates that semicore electrons are included/not included). All values are in eV and are referred to the DFT valence band top. The last row reports the difference between the SR and the FR gap for each case considered.

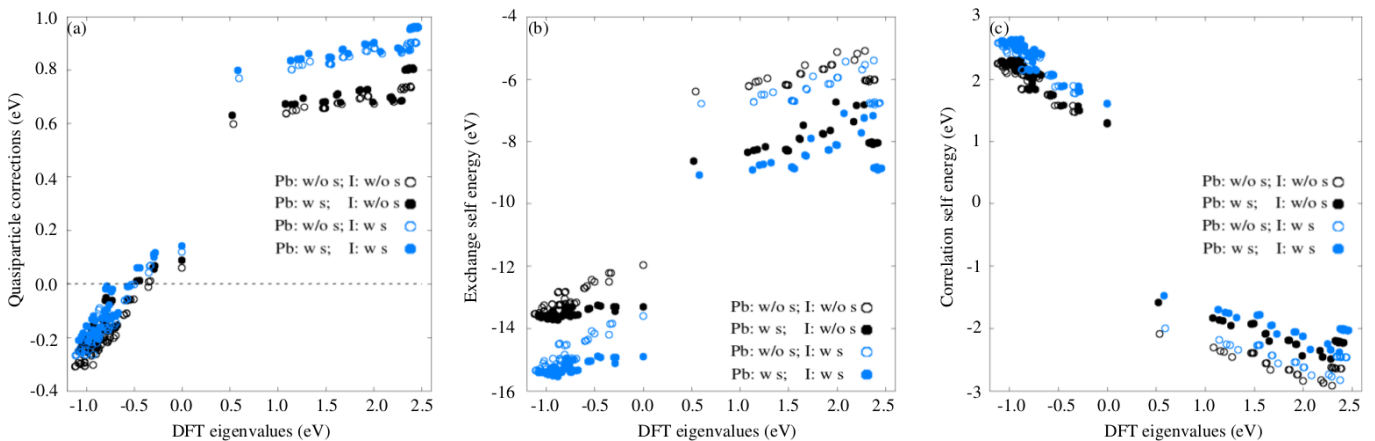


FIG. 3: (a) Fully-relativistic quasiparticle corrections of the DFT/LDA band gap, (b) the exchange self-energy, and (c) the correlation self-energy of states near the band edges and throughout the Brillouin zone, as a function of DFT/LDA eigenvalues. The key to the symbols and the calculation parameters are the same as in Fig. 2.

damped by the energy separation between valence and semicore (Pb-5*d* and I-4*d* states lie around 15 eV and 40 eV below the valence band top, respectively).

In Fig. 3(b) and (c) we can see that, in line with the above reasoning, the effect of semicore states is most pronounced (~ 1 eV) in the exchange part of the self-energy, and somewhat smaller for the correlation part (~ 0.5 eV). Focusing on the exchange part [Fig. 3(b)] we note that the bottom of the conduction band is mostly affected by the Pb-5*d* electrons. This is consistent with the predominant Pb-6*p* character of those states.^{37,46} Similarly the corrections near the top of the valence band are affected both by Pb-5*d* and I-4*d* semicore states, in line with the observation that those states carry both Pb-6*s* and I-5*p*

character.^{37,46}

Taken together these results indicate that GW quasiparticle corrections are sensitive to the explicit inclusion of semicore electrons in the valence, and this may result in band gap variations around 15%.

As a side note we mention that in all the calculations discussed in this section we obtained a quasiparticle renormalization factor of 0.80 ± 0.07 (both for SR and FR calculations, and irrespective of the valence configuration).

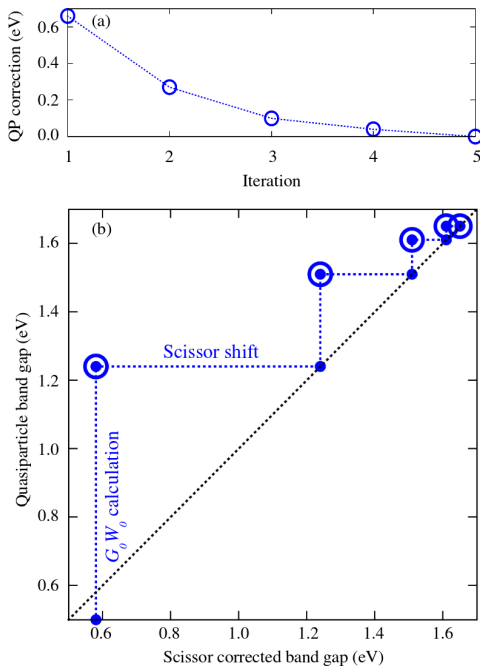


FIG. 4: (a) Convergence of the self-consistent scissor correction to the band gap of MAPbI₃ with the number of iterations. The first iteration corresponds to a G_0W_0 calculation using DFT/LDA eigenstates and eigenvalues (i.e. no scissor correction). (b) Evolution of the quasiparticle band gap of MAPbI₃ throughout the SS- GW iterative procedure. The blue dotted lines show the progression of the calculation at each iteration: the vertical blue lines represent the G_0W_0 calculation performed at each iteration, while the horizontal blue lines are the scissor shifts applied at each iteration. The iterative procedure stops when the G_0W_0 correction vanishes, that is when the small and large circle do coincide on the black dotted line.

C. Effect of self-consistent scissor correction

For clarity in this section we only present results obtained from fully relativistic GW calculations including both Pb-5*d* and I-4*d* semicore electrons in the valence.

Figure 4(a) shows the convergence of the quasiparticle correction to the band gap at each iteration of the self-consistent scissor procedure described in Sec. II B. The SS- GW procedure converges after five iterations, at which point the band gap correction becomes smaller than 10 meV.

A visual representation of the self-consistent procedure is provided in Fig. 4(b), where we plot the quasiparticle band gap vs. the scissor-corrected gap of the previous iteration. We note the close similarity of this plot with those obtained in previous $GW+U$ calculations on different systems.^{64,65}

Our final self-consistent value of the quasiparticle band gap of MAPbI₃ is 1.65 eV.

	Present work		Previous GW		Experiment
	G_0W_0	SS- GW	G_0W_0	QSGW	
SR	2.51		2.68 ^a , 2.73 ^b		
FR	1.24	1.65	1.67 ^a , 1.27 ^b	1.67 ^b	1.62-1.64 ^c

^aRef. 58.

^bRef. 62.

^cRef. 31.

TABLE II: Comparison between our calculated quasiparticle band gaps of MAPbI₃, obtained here within the G_0W_0 or the self-consistent scissor (SS- GW) approach, and previously reported values (in eV). The measured optical gap is estimated by using the midpoint of the absorption onset in the optical spectra of Ref. 31 [curves at 4.2 K in Fig. 1(a) and Fig. 1(b) of Ref. 31]. ‘ G_0W_0 ’ indicate standard perturbative GW calculations, ‘QSGW’ indicates quasiparticle self-consistent GW calculations. ‘SR’ and ‘FR’ stand for scalar- and fully-relativistic calculations, respectively.

V. DISCUSSION

Table II reports our best results for the quasi-particle band gap of MAPbI₃. For completeness we provide both scalar- and fully-relativistic G_0W_0 results and the SS- GW gap in the fully relativistic case.

In the same table we compare our results with the calculations of Refs. 58 and 62, and with the measured optical gap reported in Ref. 31.

Our G_0W_0 SR band gaps are in good agreement with previous calculations, and also overestimate the band gap with respect to experiment by up to 1 eV due to the neglect of relativistic effects. FR calculations including spin-orbit coupling yield much a improved G_0W_0 gap, in good agreement with the G_0W_0 value reported in Ref. 62. However, we should point out that this agreement is somewhat fortuitous, since in Ref. 62 the quasi-particle renormalization (which in our case is $Z = 0.8$) was not taken into account. We speculate that the agreement may be due to the fact that the authors of Ref. 62 considered a cubic MAPbI₃ structure which is known to have a slightly smaller gap than its orthorhombic counterpart. Our band gap obtained within the self consistent scissor approach (1.65 eV) matches well the quasiparticle self-consistent GW (QSGW) band gap reported in Ref. 62 (1.67 eV). This is not too surprising since the energy-dependence of the quasiparticle corrections for MAPbI₃ is very smooth, as in standard semiconductors like silicon [see Fig. 3(a)]. This should be an indication that our simple self-consistent scissor should be able to mimic more elaborate self-consistent procedures.

The validity of the SS- GW approach is especially interesting in the wider context of predicting from first principles the band gap of a variety of hybrid perovskites. In fact this approach is simple, transparent, and effective, and its computational cost is essentially negligible

once the initial G_0W_0 calculation has been performed. This procedure could also be used as a way to gauge the reliability of the perturbative treatment, by simply comparing the initial G_0W_0 gap with the final SS- GW gap: a significant discrepancy between these values may signal the need to go beyond the standard G_0W_0 theory.

When we compare our results with the calculations of Ref. 58 we find that our FR gap (1.24 eV) is about 0.4 eV smaller than their value (1.67 eV), and that the latter result is very close to our SS- GW gap. This apparently puzzling situation can be rationalized by noting that in Ref. 58 the Green's function is fully relativistic, but the screened Coulomb interaction is calculated at the scalar relativistic level. This choice implies that the W_0 of Ref. 58 was obtained starting from a DFT/LDA gap which was artificially increased by the neglect of spin-orbit effects. In doing so the W_0 of Ref. 58 was obtained using a DFT/LDA band gap which is close to our scissor-corrected gap. In other words the choice of Ref. 58 of neglecting spin-orbit effects in W_0 acts as an 'effective scissor correction'. This observation nicely reconciles the apparent discrepancy between the results of Ref. 58 and Ref. 62.

Moving on to a comparison with experiment, since we are studying the low-temperature orthorhombic structure at $T = 0$ we consider the gap measured in Ref. 31 at 4.2 K. The exciton binding energy estimated in Ref. 31 is 55–20 meV, and the measured optical gap is 1.62–1.64 eV. These values are in very good agreement with our calculated gap of 1.65 eV, especially if we account for the width of the optical lineshape.

At this point we should mention that our calculations do not include the effect of the zero-point renormalization induced by the electron-phonon interaction.⁹² However, while these effects can be large in light elements like carbon,^{93–95} in the case of MAPbI₃ they are expected to be small due to the heavy masses of Pb and I.

VI. CONCLUSIONS

In this manuscript we reported a systematic study of the quasi-particle band gap of the hybrid organic-inorganic lead halide perovskite MAPbI₃ (MA = CH₃NH₃⁺), using GW many-body perturbation theory.

We placed an emphasis on the reliability and reproducibility of our calculations by providing comprehensive convergence tests, as well as a detailed assessment of the accuracy of our calculations.

We found that the explicit inclusion of semicore Pb-5*d* and I-4*d* electrons in the valence manifold is important in order to obtain a quantitatively accurate band gap. In

fact, the neglect of the semicore states can induce errors in the gap of the order of 15%.

We demonstrated that the converged G_0W_0 band gap including semicore electrons and spin-orbit coupling underestimates significantly (by 0.4 eV) the experimental optical gap of MAPbI₃. In order to address this deficiency we tested a simple self-consistent scissor correction approach (SS- GW). We demonstrated that this simple method can achieve very good agreement with experiment and with more elaborate self-consistent GW schemes.

Our calculations allowed us to clarify the apparent discrepancy between two previous GW calculations of the band gap of MAPbI₃.^{58,62} In particular we showed that the calculations of Ref. 58, by neglecting spin-orbit effects in the evaluation of the screened Coulomb interaction, effectively incorporate an element of self-consistency. After taking this aspect into account our calculations and those of Refs. 58,62 turn out to be in good agreement.

Using self-consistent scissor approach we obtained a best-estimate for the band gap (1.65 eV), which is very close to available experimental data (1.62–1.64 eV).

Our present findings suggest that the SS- GW approach may find wider application in the first-principles prediction of the band gap of related perovskites. This could be important in view of developing automated high-throughput computational screening strategies relying on GW calculations.

Given the well known excitonic properties of MAPbI₃,³¹ future work should focus on a systematic computational study of the optical absorption spectrum within the Bethe-Salpeter formalism. Furthermore it will be important to carefully assess the impact of electron-phonon interactions on the electronic and optical properties of MAPbI₃.

It is hoped that the detailed analysis presented in this work will serve as a reliable starting point for future studies of the electronic and optical properties of this exciting material and the wider family of metal-halide hybrid perovskites.

Acknowledgments

This work was supported by the European Research Council (EU FP7 / ERC grant no. 239578), the UK Engineering and Physical Sciences Research Council (Grant No. EP/J009857/1) and the Leverhulme Trust (Grant RL-2012-001). Calculations were performed at the Oxford Supercomputing Centre and at the Oxford Materials Modelling Laboratory. All structural models were rendered using VESTA⁹⁶.

¹ A. Kojima, K. Teshima, Y. Shirai, and M. T., J. Am. Chem. Soc. **131**, 6050 (2009).

² H. Zhou, Q. Chen, G. Li, S. Luo, T. Song, H.-S. Duan, Z. Hong, J. You, Y. Liu, and Y. Yang, Science **345**, 542

- (2014).
- ³ B. O'Regan and M. Grätzel, *Nature* **353**, 737 (1991).
 - ⁴ H.-S. Kim, C. R. Lee, J.-H. Im, K.-B. Lee, T. Moehl, A. Marchioro, S.-J. Moon, R. Humphry-Baker, Y. J.-H., J. E. Moser, et al., *Sci. Rep.* **2**, 591 (2012).
 - ⁵ M. M. Lee, J. Teuscher, T. Miyasaka, T. N. Myrakami, and H. J. Snaith, *Science* **338**, 643 (2012).
 - ⁶ M. Green, A. Ho-Baillie, and H. J. Snaith, *Nature Photonics* **8**, 506 (2014).
 - ⁷ N.-G. Park, *Materials Today* **365**, 1 (2014).
 - ⁸ J. H. Heo, S. H. Im, J. H. Noh, T. N. Mandal, L. C.-S., J. A. Chang, Y. H. Lee, H. Kim, A. Sarkar, M. K. Nazeeruddin, et al., *Nature Photonics* **7**, 486 (2013).
 - ⁹ J. Burschka, N. Pellet, S.-J. Moon, R. Humphry-Baker, P. Gao, M. K. Nazeeruddin, and M. Grätzel, *Nature* **499**, 316 (2013).
 - ¹⁰ J. H. Noh, S. H. Im, T. N. Heo, J. H. end Mandal, and S. I. Seok, *Nano Lett.* **13**, 1764 (2013).
 - ¹¹ J. M. Ball, M. M. Lee, A. Hey, and H. J. Snaith, 6 p. 1739 (2013).
 - ¹² P. Docampo, J. M. Ball, M. Darwich, G. E. Eperon, and H. J. Snaith, *Nature Commun.* **4**, 2761 (2013).
 - ¹³ M. Liu, M. B. Johnston, and H. J. Snaith, *Nature* **501**, 395 (2013).
 - ¹⁴ D. Liu and T. L. Kelly, *Nature. Photon.* **8**, 133 (2014).
 - ¹⁵ G. E. Eperon, V. M. Burlakov, A. Goriely, and H. J. Snaith, *Adv. Func. Mater.* **24**, 151 (2014).
 - ¹⁶ Q. Chen, H. Zhou, Z. Hong, S. Luo, H.-S. Duan, H.-H. Wang, Y. Liu, L. Gang, and Y. Yang, *J. Am. Chem. Soc.* **136**, 622 (2014).
 - ¹⁷ M. He, D. Zheng, M. Wang, C. Lin, and Z. Lin, *J. Mater. Chem. A* **2**, 5994 (2014).
 - ¹⁸ S. Bai, Z. Wu, X. Wu, Y. Jin, N. Zhao, Z. Chen, Q. Mei, X. Wang, Z. Ye, T. Song, et al., *Nano Research* (2014).
 - ¹⁹ S. Gamliel and L. Etgar, *RSC Adv.* **4**, 29012 (2014).
 - ²⁰ G. E. Eperon, V. M. Burlakov, A. Goriely, and H. J. Snaith, *ACS Nano* **8**, 591 (2014).
 - ²¹ S. A. Kulkarni, T. Baikie, P. P. Boix, N. Yantara, N. Mathews, and S. Mhaisalkar, *J. Mater. Chem. A* **2**, 9221 (2014).
 - ²² C. Roldan-Carmona, O. Malinkiewicz, R. Betancur, G. Longo, C. Mombona, F. Jaramillo, and H. J. Bolink, *Energ. Env. Sci.* **7**, 2968 (2014).
 - ²³ M. H. Kumar, N. Yantara, S. Dharani, M. Grätzel, S. Mhaisalkar, P. D. Boix, and N. Mathews, *Chem. Commun.* **49**, 11089 (2013).
 - ²⁴ J. You, Z. Hong, Y. M. Yang, Q. Chen, M. Cai, T.-B. Song, C.-C. Chen, S. Lu, Y. Liu, H. Zhou, et al., *ACS Nano* **8**, 1674 (2014).
 - ²⁵ C. Roldan-Carmona, O. Malinkiewicz, A. Soriano, G. M. Espallargas, A. Garcia, P. Reinecke, T. Kroyer, M. I. Dar, M. K. Nazeeruddin, and H. J. Bolink, *Energ. Env. Sci.* **7**, 994 (2014).
 - ²⁶ N. K. Noel, S. D. Stranks, A. Abate, C. Wehrenfennig, S. Guarnera, A.-A. Haghighirad, A. Sadhanala, G. E. Eperon, S. K. Pathak, M. Johnston, et al., *Energ. Env. Sci.* **7**, 3061 (2014).
 - ²⁷ F. Hao, C. C. Stoumpos, D. H. Cao, R. P. H. Chang, and M. G. Kanatzidis, *Nature Photonics* **8**, 489 (2014).
 - ²⁸ A. Poglitsch and D. Weber, *J. Chem. Phys.* **87**, 6373 (1987).
 - ²⁹ T. Baikie, Y. Fang, J. M. Kadro, M. Schreyer, F. Wei, S. G. Mhaisalkar, M. Grätzel, and T. J. White, *J. Chem. Mater.* **A 1**, 5628 (2013).
 - ³⁰ C. C. Stoumpos, C. D. Malliakas, and M. G. Kanatzidis, *Inorg. Chem.* **52**, 9019 (2013).
 - ³¹ V. D'Innocenzo, G. Grancini, M. J. P. Alcocer, A. R. S. Kandada, S. D. Stranks, M. M. Lee, G. Lanzani, H. J. Snaith, and A. Petrozza, *Nature Commun.* **5**, 3586 (2014).
 - ³² J. Knutson, J. D. Martin, and D. B. Mitzi, *Inorg. Chem.* **44**, 4699 (2005).
 - ³³ G. E. Eperon, S. D. Stranks, C. Menelaou, M. Johnston, L. M. Hertz, and H. J. Snaith, *Energ. Env. Sci.* **7**, 982 (2014).
 - ³⁴ A. Amat, E. Mosconi, E. Ronca, C. Quarti, P. Umari, K. Nazeeruddin, Md, M. Grätzel, and F. De Angelis, *Nano Lett.* **14**, 3508 (2014).
 - ³⁵ H. Choi, J. Jeong, H.-B. Kim, S. Kim, B. Walker, G.-H. Kim, and J. Y. Kim, *Nano Energy* **117**, 80 (2014).
 - ³⁶ N. Pellet, P. Gao, G. Gregori, T.-Y. Yang, M. K. Nazeeruddin, J. Maier, and M. Grätzel, *Angew. Chem.* **53**, 3151 (2014).
 - ³⁷ M. R. Filip, G. Eperon, H. J. Snaith, and F. Giustino, <http://arxiv.org/abs/1409.6478> (2014).
 - ³⁸ F. Hao, C. C. Stoumpos, R. P. H. Chan, and M. G. Kanatzidis, *J. Am. Chem. Soc.* **136**, 8094 (2014).
 - ³⁹ S. D. Stranks, G. E. Grancini, G. Menelaou, C. Alcocer, M. J. P. Leijtens, H. L. M., A. Petrozza, and H. J. Snaith, *Science* **342**, 341 (2013).
 - ⁴⁰ C. Wehrenfennig, G. E. Eperon, M. B. Johnston, H. J. Snaith, and L. M. Herz, *Adv. Mater.* **26**, 1584 (2013).
 - ⁴¹ G. Xing, N. Mathews, S. Sun, S. S. Lim, Y. M. Lam, M. Grätzel, S. Mhaisalkar, and S. T. C., *Science* **342**, 344 (2013).
 - ⁴² A. Marchioro, J. Teuscher, D. Friedrich, M. Kunst, R. van der Krol, T. Moehl, M. Grätzel, and J. E. Moser, *Nature Photonics* **8**, 250 (2014).
 - ⁴³ H. Oga, A. Saeki, Y. Ogomi, S. Hayase, and S. Seki, *J. Am. Chem. Soc.* **136**, 13818 (2014).
 - ⁴⁴ S. D. Stranks, V. M. Burlakov, T. Leijtens, J. M. Ball, A. Goriely, and H. J. Snaith, *Phys. Rev. Applied* **2**, 034007 (2014).
 - ⁴⁵ V. W. Bergmann, S. A. L. Weber, F. J. Ramos, M. K. Nazeeruddin, M. Grätzel, D. Li, A. L. Domanski, I. Lieberwirth, S. Ahmad, and R. Berger, *Nature Commun.* (2014).
 - ⁴⁶ A. Filippetti, P. Delugas, and A. Mattoni, *J. Phys. Chem. C*, in press (2014).
 - ⁴⁷ P. Hohenberg and W. Kohn, *Phys. Rev.* **136**, B864 (1964).
 - ⁴⁸ E. Mosconi, A. Amat, M. K. Nazeeruddin, M. Grätzel, and F. De Angelis, *J. Phys. Chem. C* p. 117 (2013).
 - ⁴⁹ R. Lindblad, D. Bi, B. Park, J. Oscarsson, M. Gorgoi, H. Sigbahn, M. Odelius, E. M. J. Johansson, and H. Rensmo, *J. Phys. Chem. Lett.* **5**, 648 (2014).
 - ⁵⁰ E. Mosconi, E. Ronca, and F. De Angelis, *J. Phys. Chem. Lett.* **5**, 2619 (2014).
 - ⁵¹ V. Roiati, E. Mosconi, A. Listorti, S. Colella, G. Gigli, and F. De Angelis, *Nano Lett.* **14**, 2168 (2014).
 - ⁵² I. Borriello, G. Cantele, and D. Ninno, *Phys. Rev. B* **77**, 235214 (2008).
 - ⁵³ F. Brivio, A. B. Walker, and A. Walsh, *Appl. Phys. Lett.* **1**, 042111 (2013).
 - ⁵⁴ G. Grancini, S. Marras, M. Prato, C. Giannini, F. Quarti, C. and De Angelis, M. De Bastiani, G. E. Eperon, H. J. Snaith, L. Manna, and A. Petrozza, *J. Phys. Chem. Lett.*, in press (2014).
 - ⁵⁵ C. Quarti, G. Grancini, E. Mosconi, P. Bruno, J. M. Ball, M. M. Lee, H. J. Snaith, A. Petrozza, and F. De Angelis, *J. Phys. Chem. Lett.* **5**, 279 (2014).
 - ⁵⁶ J. M. Frost, K. T. Butler, and A. Walsh, *Appl. Phys. Lett.*

- 2, 081506 (2014).
- ⁵⁷ Y. H. Chang, C. H. Park, and K. Matsuishi, *J. Kor. Phys. Soc.* **44**, 89 (2004).
- ⁵⁸ P. Umari, E. Mosconi, and F. De Angelis, *Sci. Rep.* **4**, 4467 (2014).
- ⁵⁹ J. Even, L. Pedesseau, J.-M. Jancu, and C. Katan, *J. Phys. Chem. Lett.* **4**, 2999 (2013).
- ⁶⁰ J. Even, L. Pedesseau, J. M. Jancu, and C. Katan, *Phys. Status Solidi (RRL)* **8**, 31 (2014).
- ⁶¹ L. Hedin, *Phys. Rev.* **139**, A796 (1965).
- ⁶² F. Brivio, K. T. Butler, A. Walsh, and M. van Schilfgaarde, *Phys. Rev. B* **89**, 155204 (2014).
- ⁶³ M. van Schilfgaarde, T. Kotani, and S. Faleev, *Phys. Rev. Lett.* **96**, 226402 (2006).
- ⁶⁴ E. Kioupakis, P. Zhang, M. L. Cohen, and S. G. Louie, *Phys. Rev. B* **77**, 155114 (2008).
- ⁶⁵ C. E. Patrick and F. Giustino, *J. Phys. Condens. Matter* **24**, 202201 (2012).
- ⁶⁶ M. S. Hybertsen and S. G. Louie, *Phys. Rev. B* **34**, 5390 (1986).
- ⁶⁷ F. Aryasetiawan and O. Gunnarsson, *Rep. Prog. Phys.* **61**, 237 (1998).
- ⁶⁸ S. L. Adler, *Phys. Rev.* **126**, 413 (1962).
- ⁶⁹ N. Wiser, *Phys. Rev.* **129**, 62 (1963).
- ⁷⁰ R. W. Godby and R. J. Needs, *Phys. Rev. Lett.* **62**, 1169 (1989).
- ⁷¹ G. Onida, L. Reining, and A. Rubio, *Rev. Mod. Phys.* **74**, 601 (2002).
- ⁷² L. Martin-Samos and G. Bussi, *Comp. Phys. Commun.* **180**, 1416 (2009).
- ⁷³ F. Fuchs, J. Furthmüller, F. Bechstedt, M. Shishkin, and G. Kresse, *Phys. Rev. B* **76**, 115109 (2007).
- ⁷⁴ F. Bruneval and M. A. L. Marques, *J. Chem. Theory Comput.* **9**, 324 (2013).
- ⁷⁵ F. Caruso, P. Rinke, X. Ren, M. Scheffler, and A. Rubio, *Phys. Rev. B* **86**, 081102 (2012).
- ⁷⁶ F. Caruso, P. Rinke, X. Ren, A. Rubio, and M. Scheffler, *Phys. Rev. B* **88**, 075105 (2013).
- ⁷⁷ F. Giustino, M. L. Cohen, and S. G. Louie, *Phys. Rev. B* **81**, 115105 (2010).
- ⁷⁸ A. Alkauskas, P. Broqvist, F. Devynck, and A. Pasquarello, *Phys. Rev. Lett.* **101**, 106802 (2008).
- ⁷⁹ K. Noori and F. Giustino, *Adv. Func. Mater.* **22**, 5089 (2012).
- ⁸⁰ P. Gianozzi et al., *J. Phys.: Condens. Matter.* **21** (2009).
- ⁸¹ J. P. Perdew and A. Zunger, *Phys. Rev. B* **23**, 5048 (1981).
- ⁸² D. M. Ceperley and B. J. Alder, *Phys. Rev. Lett.* **45**, 566 (1980).
- ⁸³ U. von Barth and R. Car (unpublished).
- ⁸⁴ N. Troullier and J. L. Martins, *Phys. Rev. B* **43**, 1993 (1991).
- ⁸⁵ A. Marini, C. Hogan, M. Grüning, and D. Varsano, *Comp. Phys. Commun.* **180**, 1392 (2009).
- ⁸⁶ R. Sakuma, C. Friedrich, T. Miyake, S. Blügel, and F. Aryasetiawan, *Phys. Rev. B* **84**, 085144 (2011).
- ⁸⁷ F. Aryasetiawan and S. Biermann, *Phys. Rev. Lett.* **100**, 116402 (2008).
- ⁸⁸ F. Aryasetiawan and S. Biermann, *J. Phys. Condens. Matter* **21**, 064232 (2009).
- ⁸⁹ M. Rohlfing, P. Krüger, and J. Pollmann, *Phys. Rev. Lett.* **75**, 3489 (1995).
- ⁹⁰ M. L. Tiago, S. Ismail-Beigi, and S. G. Louie, *Phys. Rev. B* **69**, 125212 (2004).
- ⁹¹ M. R. Filip, C. E. Patrick, and F. Giustino, *Phys. Rev. B* **87**, 205125 (2013).
- ⁹² P. B. Allen and V. Heine, *J. Phys. C: Solid State Physics* **9**, 2305 (1976).
- ⁹³ F. Giustino, S. G. Louie, and M. L. Cohen, *Phys. Rev. Lett.* **105**, 265501 (2010).
- ⁹⁴ E. Cannuccia and A. Marini, *Phys. Rev. Lett.* **107**, 255501 (2011).
- ⁹⁵ G. Antonius, S. Pónce, P. Boulanger, M. Côté, and X. Gonze, *Phys. Rev. Lett.* **112**, 215501 (2014).
- ⁹⁶ K. Momma and F. Izumi, *J. Appl. Cryst.* **41**, 653 (2008).